



Enhanced superconductivity in $\text{Ti}_{1-x}\text{Mn}_x$ alloys through Mn doping

Ying-Jie Zhang , Qing Li ^{*}, Zhengyan Zhu, Yiwen Li, Wei Xie, and Hai-Hu Wen[†]

National Laboratory of Solid State Microstructures and Department of Physics, Center for Superconducting Physics and Materials, Collaborative Innovation Center for Advanced Microstructures, Nanjing University, Nanjing 210093, China



(Received 8 January 2023; revised 1 July 2023; accepted 7 August 2023; published 17 August 2023)

The magnetic element Mn is generally supposed to be harmful to superconductivity. However, the superconducting transition temperature of $\text{Ti}_{1-x}\text{Mn}_x$ can be enhanced from 0.4 K (elemental titanium) to about 2.1–2.8 K by doping Mn to the system. Here, we carry out systematic studies on the superconductivity and normal state properties of $\text{Ti}_{1-x}\text{Mn}_x$ alloys. With the increase of Mn doping in $\text{Ti}_{1-x}\text{Mn}_x$, we find that the system transforms from hexagonal α phase ($P6_3/mmc$) to cubic β phase ($Im\bar{3}m$), and the superconducting property changes from filamentary to bulk superconductivity. Thus we argue that the superconductivity in the α phase with dilute Mn doping is not intrinsic; it may be induced by the residual β phase embedded in the α phase. Moreover, in $\text{Ti}_{0.88}\text{Mn}_{0.12}$, we find a positive Hall coefficient with a significant reduction of charge-carrier density, which is in contrast to pure Ti where the Hall coefficient is negative. The specific-heat data of $\text{Ti}_{1-x}\text{Mn}_x$ with $x = 0.12$ can be described by the model of s -wave symmetry with a fully opened gap of 0.37 meV. Transport measurements show that it is a type-II superconductor with a relatively large value of Wilson ratio ($R_W = 3.1$) in the normal state, which suggests a moderate electron correlation in $\text{Ti}_{1-x}\text{Mn}_x$ with the β phase. The positive correlation between magnetic susceptibility and temperature, and the sudden drop of effective magnetic moment in $\text{Ti}_{1-x}\text{Mn}_x$ with $x = 0.12$ may suggest that the material shows a signature of the existence of spin fluctuations.

DOI: [10.1103/PhysRevB.108.054516](https://doi.org/10.1103/PhysRevB.108.054516)

I. INTRODUCTION

According to the earlier theoretical predictions based on the Bardeen-Cooper-Schrieffer (BCS) theory [1], the existence of magnetic ions will suppress the superconductivity in conventional superconductors [2]. For example, the superconducting transition temperature (T_c) of lanthanum will drop down from 5.6 K to about 0.6 K after doping 1 atomic percent (at. %) gadolinium [3], and similar cases occur in iron-doped molybdenum and iridium [4,5]. Thus, it has been assumed for a considerable period that we should keep away from magnetic elements when seeking new superconductors [6]. The situation has changed after the discovery of heavy fermion superconductors and iron-based high-temperature superconductors [7,8], in which the magnetic elements, such as Ce, Eu, and Fe, act as the major components to host superconductivity with unconventional properties. In some cases, superconductivity even coexists with the magnetic order [9,10]. In recent years, superconductivity has been observed in some compounds containing Cr or Mn, like CrAs and MnP [11–13]. After that, a series of chromium-based (ACr_3As_3 and $\text{A}_2\text{Cr}_3\text{As}_3$; here A is alkali metal [14–18], $\text{Pr}_3\text{Cr}_{10-x}\text{N}_{11}$ [19] and CrB_2 [20]), and manganese-based (MnSe [21], KMn_6Bi_5 [22]) superconductors have been continuously discovered. Nowadays, it is generally accepted that magnetic elements may be helpful to generate unconventional

superconductivity, and even proposed that the formation of Cooper pairs is mediated through superexchange magnetic interactions [23].

Materials containing 3d transition-metal elements are considered more likely to produce superconductivity with unconventional properties. In fact, in earlier studies [24–26], Matthias *et al.* have found that a series of solid solutions containing large amounts of 3d magnetic elements can exhibit superconductivity, such as Cr-Ru/Re, Zr-Fe/Co, and so on. Interestingly, the T_c of $\text{Ti}_{1-x}\text{M}_x$ ($M = \text{Cr}, \text{Mn}, \text{Fe}, \text{Co}$) [25] is increased by almost an order of magnitude when a certain amount of magnetic elements is dissolved in Ti ($T_c = 0.4$ K [27,28]). Despite the relatively simple elemental composition and crystal structure, Matthias *et al.* argued that the unusual enhancement of T_c in dilute $\text{Ti}_{1-x}\text{M}_x$ alloys is much more than what could be expected from the variation of electron concentration based on the BCS theory, and there may be antiferromagnetic coupling or other interactions in the system [25]. It is worth noting that the $\text{Ti}_{1-x}\text{M}_x$ alloys are always accompanied by a doping-dependent structure phase transition from hexagonal (α phase) to cubic (β phase) at ambient pressure. For comparison, pure Ti metal can only crystallize into the body-centered cubic (bcc) phase under pressures above 200 GPa [29] with a T_c over 20 K [30,31]. Hake *et al.* [32] reported the low-temperature transport properties of dilute $\text{Ti}_{1-x}\text{Mn}_x$ ($x < 2.0$ at. %) and suggested that the superconductivity in it was of a filamentary type. Cape [33] observed a localized magnetic state in the α -phase $\text{Ti}_{1-x}\text{Mn}_x$ and declared that the superconductivity of the as-cast $\text{Ti}_{1-x}\text{Mn}_x$ ($x \leq 4$ at. %) originated from the enriched β phase. Up to now, the

^{*}liqing1118@nju.edu.cn

[†]hhwen@nju.edu.cn

actual superconducting phase of $\text{Ti}_{1-x}\text{Mn}_x$ is still under debate [33–35], and the detailed physical properties of $\text{Ti}_{1-x}\text{Mn}_x$, especially in the β phase, are still lacking.

In this paper, we report a systematic study of superconductivity in $\text{Ti}_{1-x}\text{Mn}_x$ alloys with an actual Mn content range from 0 to 0.16. Thermodynamic and superconducting parameters were determined from the resistivity, magnetization, and heat-capacity measurements. It is found that the bulk superconductivity originates from the β phase. Specific-heat measurements suggest a fully gapped superconducting state in β -phase $\text{Ti}_{1-x}\text{Mn}_x$ with $2\Delta/k_B T_c$ of about 3.6. Hall resistivity measurements show a temperature-independent hole-type charge carriers in the normal states. The relatively large Ginzburg-Landau parameter ($\kappa_{GL} = 26$) and Wilson ratio ($R_W = 3.1$) indicate that $\text{Ti}_{1-x}\text{Mn}_x$ with $x = 0.12$ is a type-II superconductor with moderate electron correlation. Furthermore, there is some evidence pointing to possible antiferromagnetic spin fluctuations in the normal state; for example, the magnetic susceptibility rises gradually with increasing temperature in high-temperature region in $\text{Ti}_{1-x}\text{Mn}_x$ with $x = 0.12$ and a sudden drop of effective magnetic moment observed in the β phase. Considering the sign change and significant reduction in carrier concentrations, and the abnormal magnetization behavior in the β -phase $\text{Ti}_{1-x}\text{Mn}_x$, we may expect that the enhanced superconductivity in $\text{Ti}_{1-x}\text{Mn}_x$ through Mn doping may have some unusual origins.

II. EXPERIMENTAL DETAILS

$\text{Ti}_{1-x}\text{Mn}_x$ alloys were prepared by an arc-melting method utilizing a water-cooled copper hearth and a tungsten electrode [36]. Stoichiometric amounts of high-purity Mn (99.99%; Alfa Aesar) and Ti (99.9%; Alfa Aesar) with a total weight of 0.8 g were ground, pelletized, and placed in an arc-melting furnace filled with pure argon. Each sample was remelted at least three times and the ingot was inverted upside down after each melt to improve the homogeneity. Because the boiling point of Mn (2150 °C) is much smaller than Ti (3260 °C), the weight losses of $\text{Ti}_{1-x}\text{Mn}_x$ during the arc-melting process should mainly originate from Mn, and it is generally about 3–7 wt %.

The crystal structure of $\text{Ti}_{1-x}\text{Mn}_x$ alloys was identified by powder x-ray diffraction (XRD) with Cu $K\alpha$ radiation (Bruker; D8 Advance diffractometer; $\lambda = 1.541 \text{ \AA}$). The crystal structure of $\text{Ti}_{1-x}\text{Mn}_x$ shown in Fig. 1 is made using VESTA [37]. The micrographs and the chemical composition analysis were taken by a Phenom ProX scanning electron microscope (SEM) with an accelerating voltage of 15 kV. The electrical resistivity and heat-capacity data were collected on a physical property measurement system (Quantum Design). The Hall resistance was measured using a six-probe method. The specific heat down to 0.4 K was measured by the thermal-relaxation method with an additional ^3He insert. The magnetization measurements were performed with a SQUID-VSM-7T (Quantum Design) to acquire temperature dependence of magnetic susceptibility in zero-field-cooling (ZFC) and field-cooling (FC) modes, and magnetization hysteresis loops at different temperatures.

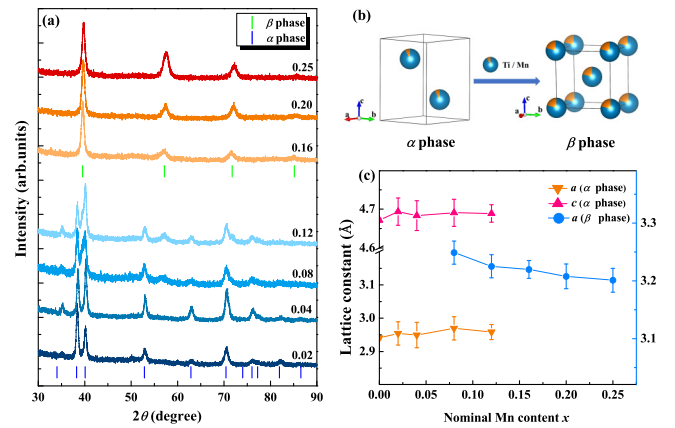


FIG. 1. (a) Room-temperature XRD patterns of $\text{Ti}_{1-x}\text{Mn}_x$; the vertical bars indicate the calculated Bragg positions of $\text{Ti}_{1-x}\text{Mn}_x$ with the α phase (blue) and the β phase (green). (b) Crystal structures of $\text{Ti}_{1-x}\text{Mn}_x$ with the α phase (left) and the β phase (right). (c) Calculated lattice parameters as a function of nominal Mn content for $\text{Ti}_{1-x}\text{Mn}_x$ alloys.

III. RESULTS AND DISCUSSION

A. Crystal structure and composition analysis

Figure 1(a) presents room-temperature powder XRD patterns of $\text{Ti}_{1-x}\text{Mn}_x$ alloys with different nominal concentrations of Mn. We can see that at a lower doping level (nominal $x \leq 0.04$), $\text{Ti}_{1-x}\text{Mn}_x$ crystallizes into a hexagonal structure (α phase) with a space group of $P6_3/mmc$ (No. 194), similar to the crystal structure of Ti under ambient pressure (space group $P6_3/mmc$, $a = b = 2.95 \text{ \AA}$, $c = 4.68 \text{ \AA}$) [38]. With the increase of doping content (nominal $x \geq 0.08$), several new diffraction peaks begin to appear in XRD patterns, as indicated by the newly formed peak at around 56° , which means that a doping-induced structural phase transition occurs. When the nominal doping concentration of Mn is higher than 16 at. %, $\text{Ti}_{1-x}\text{Mn}_x$ alloys have totally transformed into the β phase as shown in the upper part of Fig. 1(a). All the observed peaks can be indexed by a body-centered cubic structure with a space group of $Im\bar{3}m$ (No. 229) and no impurity phase was detected in our measurements. The crystal structures of $\text{Ti}_{1-x}\text{Mn}_x$ with the α phase (left) and the β phase (right) are displayed in Fig. 1(b), in which the blue and orange colors represent Ti and Mn, respectively. Note that the α - to β -phase transition is a common feature in $\text{Ti}_{1-x}M_x$ ($M = \text{Cr, Mn, Fe, Co}$) alloys [25,33] and the elemental titanium can also crystallize into the β phase at megabar pressure [29]. In this work, the α -phase to β -phase transition in $\text{Ti}_{1-x}\text{Mn}_x$ has been verified from XRD patterns.

We also extract the lattice parameters of $\text{Ti}_{1-x}\text{Mn}_x$ from XRD data and present the results in Fig. 1(c). For the α phase, the lattice parameters are essentially unchanged with Mn doping, while the lattice parameters of the β phase continuously decrease with the increase of doping concentration. In the α phase, the lattice parameters of $\text{Ti}_{1-x}\text{Mn}_x$ are almost invariable with doping, which is contrary to the fact that Ti is replaced by Mn with a smaller atomic radius.

In previous literature [33], it was reported that there may be a solubility limit of Mn in α -Ti (about 0.5 at. %). Thus, we

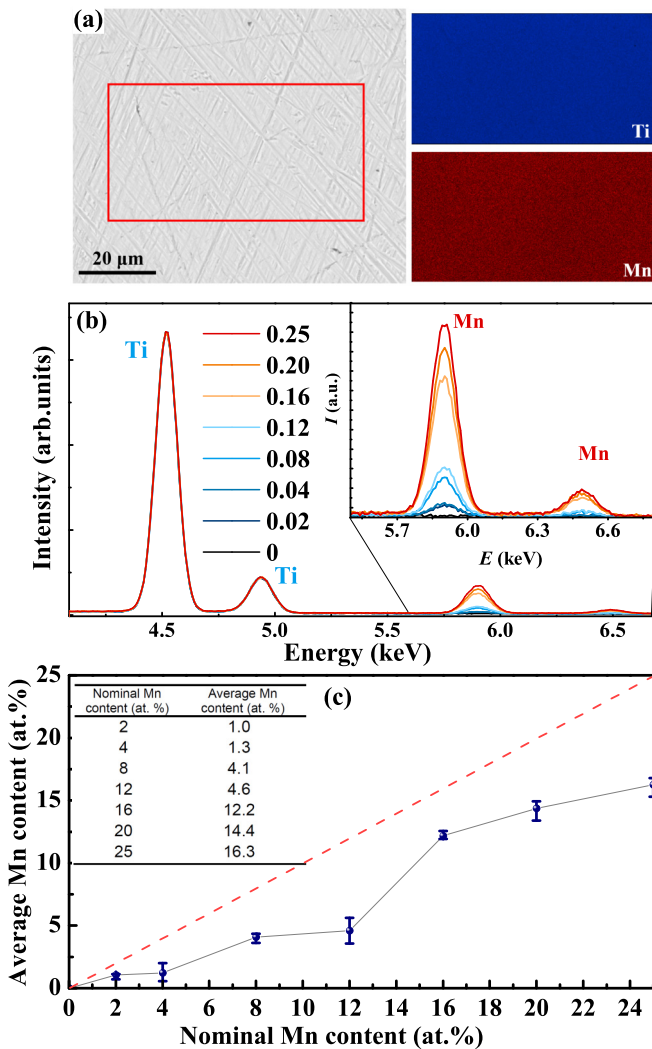


FIG. 2. (a) Representative SEM image and the corresponding element distributions of Mn (orange) and Ti (blue) in $\text{Ti}_{1-x}\text{Mn}_x$ with nominal $x = 0.25$. (b) The normalized energy dispersive spectrums of $\text{Ti}_{1-x}\text{Mn}_x$. Inset shows an enlarged view of EDS peaks of Mn with different nominal contents. (c) The evolution of average content of Mn against the nominal doping concentration in $\text{Ti}_{1-x}\text{Mn}_x$ alloys. Inset lists the actual concentration of Mn for each sample with respect to the nominal concentration.

performed the chemical composition analysis on $\text{Ti}_{1-x}\text{Mn}_x$ to see the actual concentration of Mn in these alloys. Figure 2(a) presents a representative SEM image with backscattered electron mode and the corresponding EDS mapping scans of the sample with the nominal $x = 0.25$. Scratches on the sample surface are caused by physical cuts and polishing. The relatively uniform distribution of Ti and Mn indicates Mn has been successfully doped into the sample, as shown in the right part of Fig. 2(a). The actual element composition of $\text{Ti}_{1-x}\text{Mn}_x$ with nominal $x = 0.25$ is Ti : Mn = 84 : 16, which means that there is a non-negligible volatilization of Mn during the arc-melting process. To clarify the actual doping concentration of Mn in different samples, we present the typical EDSs of $\text{Ti}_{1-x}\text{Mn}_x$ in Fig. 2(b), in which the spectrums are normalized with the peak with the highest intensity of Ti at around

4.5 keV. As shown in the inset of Fig. 2(b), there is indeed a certain solubility limit of Mn in the α -phase region (nominal $x < 0.16$), and the actual concentration of Mn undergoes a steep rise on the boundary between the α phase and the β phase.

We calculated the atomic concentration of Mn in $\text{Ti}_{1-x}\text{Mn}_x$ and the average doping values from EDS measurements are plotted against the nominal doping concentration as shown in Fig. 2(c). Error bars show the variation of the actual content of Mn with different EDS scans. We found that the actual concentration of Mn increases like steps. For nominal $x \leq 0.04$, the actual Mn content is only about 1 at. %, which is basically consistent with the previous phase diagram [33]. In the nominal doping range from 0.08 to 0.16, the actual doping content reaches the second step level (about 4 at. %). Actually, this doping range corresponds to the formation of the β phase as evident from x-ray diffraction data in Fig. 1(a). Therefore, we may attribute the second step level of Mn doping concentration in Fig. 2(c) to the formation of the β phase in the matrix of the α phase, in which Mn has a higher solubility. Later, with an overall transformation of $\text{Ti}_{1-x}\text{Mn}_x$ into the β phase (nominal $x \geq 0.16$), the average content of Mn increased for the third time. However, it should be pointed out that there is always a certain deviation between the average and the nominal content in all samples. Considering the lower concentration of Mn in the melted samples, we believe that the weight losses of Mn during the arc-melting process are dominating, which may be due to the easier volatilization of Mn. In the inset of Fig. 2(c), we give a table to illustrate the relationship between the nominal and the actual Mn content in our samples. In the following discussion, we renamed the sample according to its actual Mn content.

B. Superconducting properties and phase diagram

Figures 3(a) and 3(b) display the resistivity and magnetic susceptibility as a function of temperature of $\text{Ti}_{1-x}\text{Mn}_x$ alloys. In order to clearly show the behavior of temperature-dependent resistivity in the normal state, we present the temperature-dependent $\rho/\rho_{300\text{K}}$ in Fig. 3(a), and summarize the doping-dependent $\rho_{5\text{K}}/\rho_{300\text{K}}$ and room-temperature resistivity ($\rho_{300\text{K}}$) of $\text{Ti}_{1-x}\text{Mn}_x$ in Fig. 3(c). In α -phase dominated $\text{Ti}_{1-x}\text{Mn}_x$ ($x \leq 0.05$), the ρ - T curves behave as a normal metal with Fermi-liquid properties, whereas the $\rho_{300\text{K}}$ and the inverse of residual resistivity ($\rho_{5\text{K}}/\rho_{300\text{K}}$) both increase progressively with the increasing of doping concentration. After entering the β phase ($x \geq 0.12$), $\text{Ti}_{1-x}\text{Mn}_x$ transforms from a good metal to a weak insulating behavior, similar to the situation in NbTi [39] and some high-entropy alloys [40] with bcc structure. It is found that the value of $\rho_{5\text{K}}/\rho_{300\text{K}}$ increases about six times from α phase to β phase and remains almost unchanged after reaching 1, which is probably due to the substantial reduction of the electron mean free path caused by disorders or other defects via chemical doping [36,41].

Now let us focus on the low-temperature superconducting transitions. Elemental titanium is a good metal with T_c of about 0.4 K [27,28]. With a small amount of Mn doping ($0.01 \leq x \leq 0.04$), as shown in the inset of Fig. 3(a), a rather broad resistive transition with an onset transition

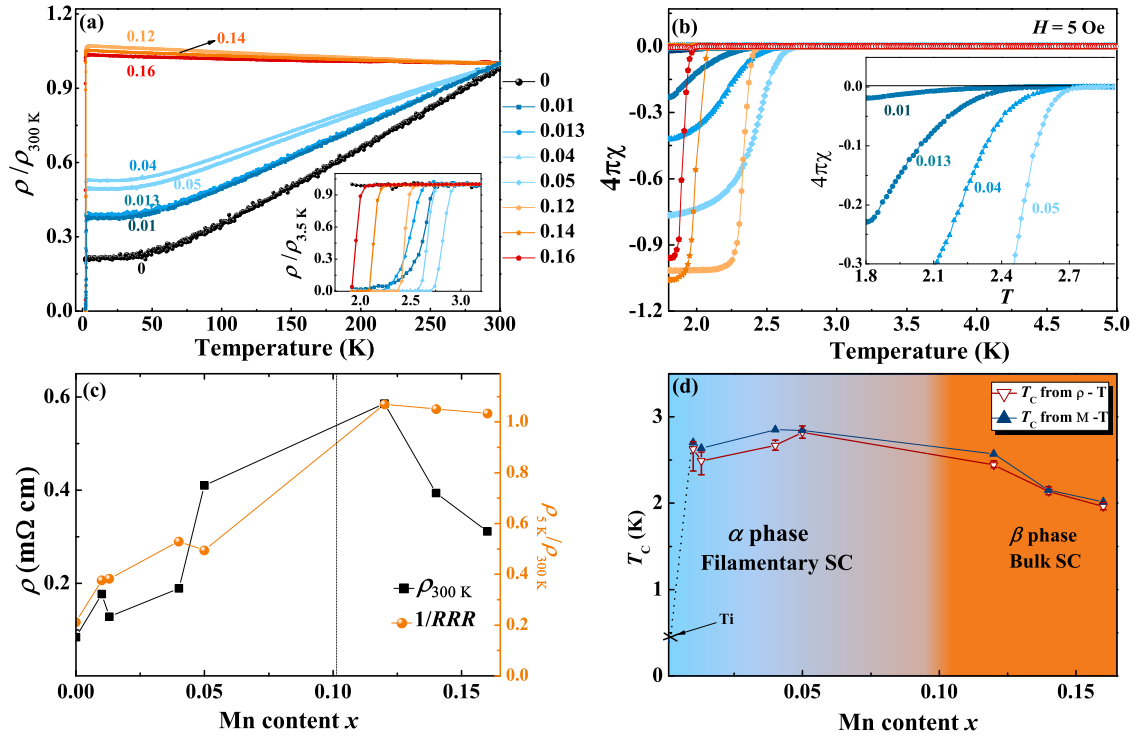


FIG. 3. (a) Normalized temperature dependence of resistivity ($\rho/\rho_{300\text{ K}} - T$) of $\text{Ti}_{1-x}\text{Mn}_x$ from 2 to 300 K. Inset shows the enlarged view of superconducting transitions. (b) Temperature dependence of magnetic susceptibility of $\text{Ti}_{1-x}\text{Mn}_x$ alloys with both ZFC mode (solid symbol) and FC mode (hollow symbol), and the applied magnetic field is 5 Oe. Inset shows the enlarged view of the magnetization curves measured in ZFC mode with low Mn content ($x \leq 0.05$). (c) The evolution of room-temperature resistivity ($\rho_{300\text{ K}}$) and $\rho_{5\text{ K}}/\rho_{300\text{ K}}$ with different Mn content. (d) Phase diagram of $\text{Ti}_{1-x}\text{Mn}_x$; the values of T_c are extracted from resistivity and magnetization curves, respectively. Error bars of resistivity measurements correspond to the transition width.

temperature of about 2.5–2.8 K is observed, which is consistent with the previous report on the dilute superconducting $\text{Ti}_{1-x}\text{Mn}_x$ alloys with the α phase [25,32,33]. Interestingly, from the magnetization measurement as given in Fig. 3(b), we find that the superconducting shielding fractions of $\text{Ti}_{1-x}\text{Mn}_x$ with the α phase are relatively small (about 1% for $x = 0.01$), and the superconducting transition is broad as well. To show the superconducting transition clearly, we also present the temperature-dependent magnetic susceptibility with ZFC mode near T_c in the inset of Fig. 3(b). Note that the superconducting fractions of $\text{Ti}_{1-x}\text{Mn}_x$ are corrected by the calculated demagnetization factor N [42]. We can see that the superconducting fraction increases with the increase of Mn doping concentration. With more Mn doping ($x \geq 0.12$), the superconducting transition becomes sharper when the material has totally transformed into the β phase and the superconducting shielding fractions are around 100%.

Combined with the results from magnetization and resistivity measurements, we tend to believe that the superconductivity in $\text{Ti}_{1-x}\text{Mn}_x$ with the α phase is filamentary and the actual superconducting component most likely originates from the residual β phase. The latter may exist in a meshlike acicular distribution of extremely fine layers or filaments separating α platelets or along parent grain boundaries as visualized in Ref. [25]. With this kind of microstructure, the zero resistance and visible superconducting shielding fractions (20% for $x = 0.013$) in the α phase are also reasonable. We summarize our experimental results and present a superconducting phase

diagram of $\text{Ti}_{1-x}\text{Mn}_x$ alloys in Fig. 3(d). T_c is determined by the temperature with a criterion of 50% of normal-state resistance ($\rho_{5\text{ K}}$), or at the onset temperature for superconductivity observed in the ZFC magnetization measurements. At the low doping concentration with $x \leq 0.05$, $\text{Ti}_{1-x}\text{Mn}_x$ alloys exhibit filamentary superconductivity with an almost constant value of T_c . However, for samples with $x \geq 0.12$, they exhibit the properties of bulk superconductivity and the T_c continuously decreases with the increase of Mn doping concentration.

C. Normal-state magnetic susceptibility and Hall resistivity

To clarify the effect of the magnetic moment of Mn on the magnetization behavior of $\text{Ti}_{1-x}\text{Mn}_x$, we measured the temperature dependence of magnetic susceptibility ($\chi - T$) curves with an applied magnetic field of 30 kOe. Figures 4(a)–4(c) display three representative curves with the Mn doping concentrations of 0.01, 0.12, and 0.16, respectively. For $x = 0.01$ with the α phase, as shown in Fig. 4(a), the magnetic susceptibility increases with decreasing temperature in the temperature region from 300 to 2 K, exhibiting a strong upturning in the low-temperature region. This observation is consistent with the previous results reported in Ti-Mn (1 at. %) alloys [33], which was considered as evidence of the existence of local magnetic moment in the alloys of $\text{Ti}_{1-x}\text{Mn}_x$ with dilute content of Mn. However, the Curie-like upturn is significantly reduced after the compound has transformed into the β phase, as seen in Figs. 4(b) and 4(c).

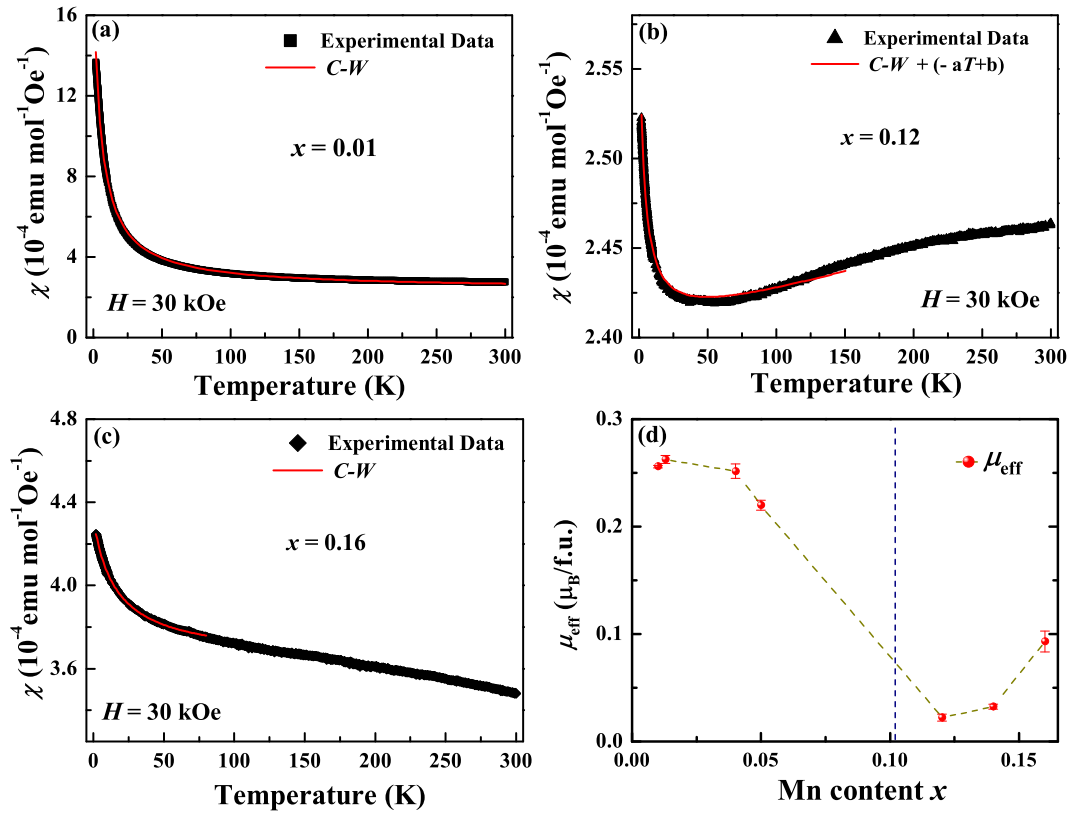


FIG. 4. Temperature dependence of magnetic susceptibility of $\text{Ti}_{1-x}\text{Mn}_x$ alloys with the Mn concentrations of (a) 0.01, (b) 0.12, and (c) 0.16, respectively. A positive correlation between temperature and magnetic susceptibility is observed in $\text{Ti}_{1-x}\text{Mn}_x$ with $x = 0.12$. (d) The doping evolution of effective magnetic moment (μ_{eff}) of $\text{Ti}_{1-x}\text{Mn}_x$ alloys with different Mn contents.

Using the Curie-Weiss law, we can fit the χ - T curves by the following equation:

$$\chi(T) = \chi(0) + \frac{C}{T - \theta}. \quad (1)$$

The first term comes from the temperature-independent contribution to the susceptibility. The second term is related to some weak magnetism arising probably from the ionic contributions. We can see that the χ - T curve of $\text{Ti}_{1-x}\text{Mn}_x$ with $x = 0.01$ can be fitted well in the whole temperature region from 2 to 300 K by Eq. (1). However, after entering the β phase, we can only use the above equation to describe the χ - T curves at low-temperature region. In $\text{Ti}_{1-x}\text{Mn}_x$ with $x = 0.12$, with the increasing temperature from 2 K, the magnetic susceptibility decreases initially and then rises gradually in the high-temperature region. The increase of magnetic susceptibility with increasing temperature is more like due to a possible antiferromagnetic order or spin fluctuations. Usually, the magnetization of antiferromagnetic materials decreases with the decrease in temperature. Note that a similar signature of the presence of spin fluctuations in χ - T curves is also observed in the Ti-V alloys [43] and α -Mn [44]. Considering the similar structure and elemental component of $\text{Ti}_{1-x}\text{Mn}_x$ and Ti-V alloys, we believe that abnormal magnetization behaviors in χ - T curves may share the same physical origins, such as spin fluctuations. Since the typical χ - T curve of antiferromagnetism decreases with increasing temperature, by simply adding a linear term with negative slope ($-aT + b$) to

Eq. (1), we can roughly fit the χ - T curve of $\text{Ti}_{1-x}\text{Mn}_x$ with $x = 0.12$ in the temperature range from 2 to 150 K as shown in Fig. 4(b).

The effective magnetic moment could be calculated through $C = \mu_0 \mu_{\text{eff}}^2 / 3k_B$, where C is the fitting parameter from Eq. (1), and the calculated μ_{eff} are shown in Fig. 4(d). In the α phase ($x \leq 0.05$), the effective magnetic moment (μ_{eff}) of $\text{Ti}_{1-x}\text{Mn}_x$ is consistent with the previous reports [33], and roughly unchanged with different doping concentrations. To our surprise, a sudden drop of μ_{eff} occurs between α and β in the phase transition. The obvious reduction of μ_{eff} in the β phase indicates that doping more Mn atoms in Ti does not induce an increase of the averaged magnetic moment, but it is even weakened. Thus, we also would like to attribute the weakened local magnetic moments in β -phase $\text{Ti}_{1-x}\text{Mn}_x$ ($x \geq 0.12$) to the possible formation of an antiferromagnetic order or spin fluctuations, which is similar to the situation in Cr-Ru/Re or Ti-V alloys [36,43,45,46]. Furthermore, we notice that there is a minimum value of μ_{eff} when $x = 0.12$, and it is exactly at the doping boundary where the phase transition occurs. Thus, we may expect the existence of a possible quantum critical point [47] in the vicinity of the transition.

In previous studies, Cape [33] argued that the superconductivity in $\text{Ti}_{1-x}\text{Mn}_x$ can be understood in terms of the changes in the electronic density state as predicted by the BCS theory [1] rather than the magnetic-interaction hypothesis claimed by Matthias *et al.* [25]. Hake *et al.* [32] have carried out Hall resistivity measurements on the

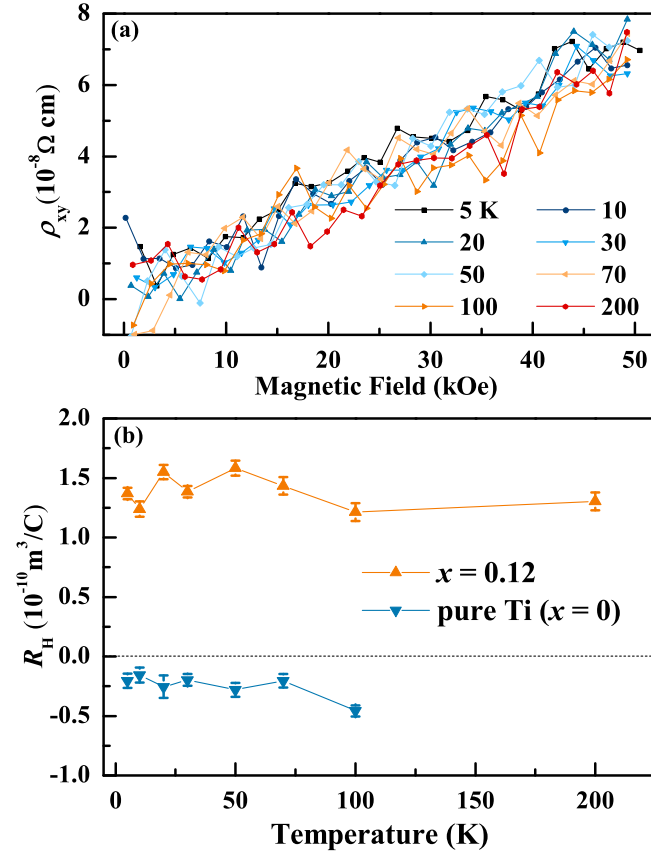


FIG. 5. (a) Hall resistivity versus magnetic field at different temperatures of the sample with $x = 0.12$. (b) Temperature dependence of the Hall coefficient of the sample with $x = 0$ and 0.12.

α -phase $\text{Ti}_{1-x}\text{Mn}_x$ ($0 \leq x \leq 0.02$), and observed a field- and temperature-dependent Hall coefficient with a value of about $-2 \times 10^5 \text{ cm}^3/\text{C}$. In order to confirm whether the doping of Mn introduces more electron-type carriers into the phase with bulk superconductivity (β phase), we performed Hall resistivity (ρ_{xy}) measurements at various temperatures on a well-defined β -phase compound $\text{Ti}_{1-x}\text{Mn}_x$ with $x = 0.12$, and present the data in Fig. 5(a). Different from the pure Ti and α -phase $\text{Ti}_{1-x}\text{Mn}_x$ ($x \leq 0.02$) [32], the Hall resistivity of $\text{Ti}_{1-x}\text{Mn}_x$ with $x = 0.12$ becomes positive, indicating that the dominant charge carriers now become hole type. In addition, the transverse resistivity curves almost overlap with each other at all measured temperatures and show a roughly linear relationship with a magnetic field.

The Hall coefficient (R_H) can be calculated through the equation $R_H = \rho_{xy}/B$, and the results are presented in Fig. 5(b). We can see that the R_H of $\text{Ti}_{1-x}\text{Mn}_x$ with $x = 0.12$ is positive and temperature independent, indicating that the β -phase $\text{Ti}_{1-x}\text{Mn}_x$ possibly falls into a single-band scenario with hole-type charge carriers. We also measured the Hall coefficient of pure Ti as a referee and put the data on the lower part of Fig. 5(b). The carrier density n can be calculated from R_H , which gives a value of about $5 \times 10^{22} \text{ cm}^{-3}$ in $\text{Ti}_{1-x}\text{Mn}_x$ with $x = 0.12$. And this value is significantly lower than that of Ti ($3 \times 10^{23} \text{ cm}^{-3}$). That is to say, the substitution of Mn for Ti not only changes the carrier type, but also reduces

the carrier concentration by almost an order of magnitude. In compressed Ti, theoretical calculations reveal the joint effect of enhanced carrier density and phonon softening, which leads to higher T_c values [30,31]. However, the carrier density of $\text{Ti}_{1-x}\text{Mn}_x$ alloys was significantly reduced by Mn doping, which is contrary to the argument of Cape [33] and BCS theory [1].

D. Specific heat and critical field

To investigate the superconductivity of $\text{Ti}_{1-x}\text{Mn}_x$ with the β phase, we performed heat-capacity measurements down to 0.4 K on $\text{Ti}_{1-x}\text{Mn}_x$ with Mn content $x = 0.12$ and 0.16 as shown in Figs. 6(a)–6(d). The specific-heat data at zero field shows a clear jump at around 2.4 K for $x = 0.12$ and 1.9 K for $x = 0.16$, respectively. The normal-state specific heat can be obtained by suppressing the superconductivity with an external magnetic field of 40 kOe as shown in Fig. 6(a). The data of the normal state can be well fitted with the Debye model, $C_P(T) = \gamma_n T + \beta T^3$ [shown as the blue dashed line in Fig. 6(c)], in which the two terms represent the contribution of electrons, and phonons, respectively. The T_c values determined from the specific-heat measurements and calculated results are listed in Table I. The Debye temperatures are calculated by using the equation $\Theta_D = (12\pi^4 k_B N_A Z / 5\beta)^{1/3}$, in which N_A and k_B represent the Avogadro constant and the Boltzmann constant, and Z is the number of atoms per formula unit. For $\text{Ti}_{1-x}\text{Mn}_x$, we use $Z = 1$. The density of states at the Fermi level is determined through the equation $N(E_F) = 3\gamma_n / (2\pi^2 k_B^2)$. The specific-heat jump ratio $\Delta C / \gamma_n T|_{T_c}$ is estimated to be about 1.3–1.4, which is consistent with the BCS prediction of 1.43 in the weak-coupling limit. By applying magnetic fields to the sample with $x = 0.12$, the specific-heat jump was gradually shifted to low temperatures in parallel with no obvious widening as shown in Fig. 6(c).

The analysis of specific-heat data can give us more information about the superconducting state of $\text{Ti}_{1-x}\text{Mn}_x$ with the β phase. Figure 6(d) shows the low-temperature specific-heat $C(T)$ curves of $\text{Ti}_{1-x}\text{Mn}_x$ with $x = 0.12$ in the superconducting state (0 kOe) and normal state (40 kOe). The superconducting state has been totally suppressed when a magnetic field of 40 kOe is applied. The C versus T curve at zero magnetic field can be fitted by the formula of specific heat based on the BCS theory. The fitting curves are shown in Fig. 6(d). We can see that a single s -wave gap or an extended s -wave gap with $\alpha = 0.125$ are suitable to describe the experimental data of $\text{Ti}_{1-x}\text{Mn}_x$ with the β phase. Here, α is the anisotropy parameter according to the extended s -wave gap. The obtained gap value is 0.37 meV, and $2\Delta/k_B T_c = 3.6$, which is a little larger but comparable to the BCS value in the weak-coupling regime. All the results from specific-heat measurements indicate that $\text{Ti}_{1-x}\text{Mn}_x$ with $x = 0.12$ may be conventional s -wave superconductor in the weak-coupling limit. By the way, in order to confirm the bulk superconductivity of β -phase $\text{Ti}_{1-x}\text{Mn}_x$, we also calculated the superconducting volume fraction from the specific-heat data through $(\gamma_n - \gamma_0) / \gamma_n$, where γ_0 is the specific-heat coefficient at zero temperature in the superconducting state and γ_n is the normal-state electronic specific-heat coefficient. And the calculated superconducting volume fractions are both

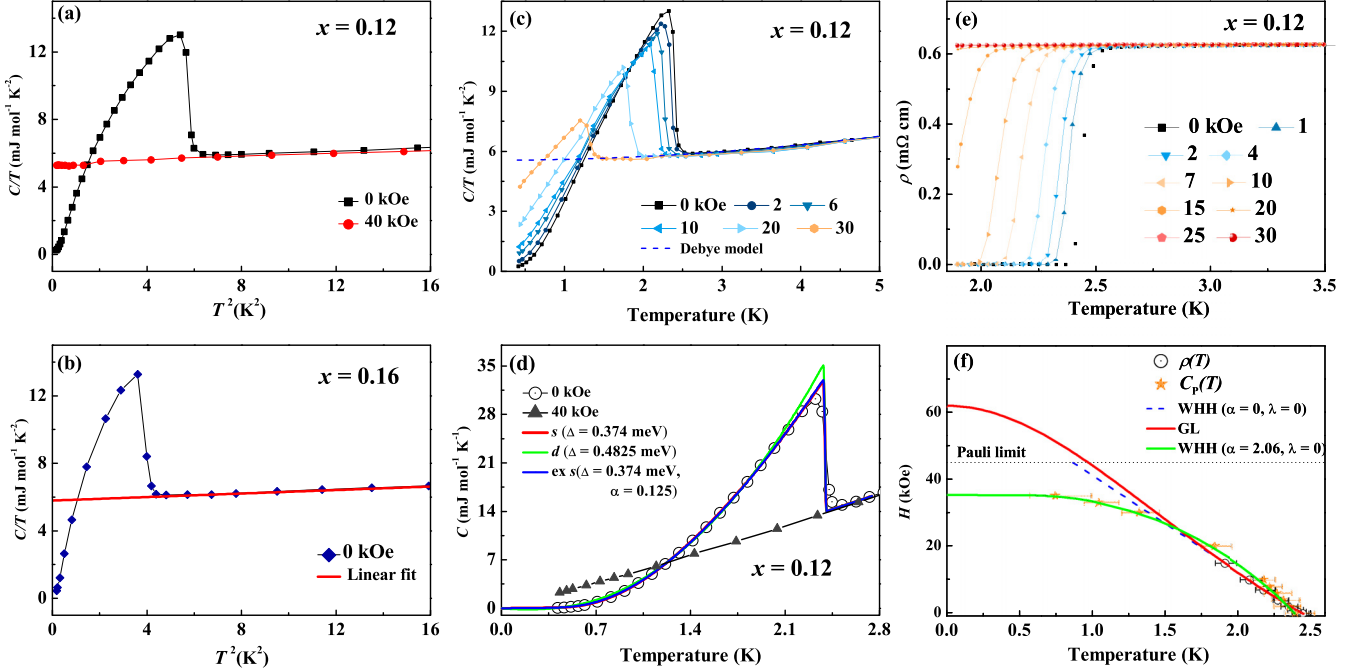


FIG. 6. (a), (b) C/T as a function of T^2 for $x = 0.12$ (0 and 40 kOe) and $x = 0.16$ (0 kOe). The red curve in (b) is the linear fit of the normal-state specific-heat data considering the Debye model. (c) Low-temperature heat capacity of $\text{Ti}_{1-x}\text{Mn}_x$ with Mn content $x = 0.12$ under different magnetic fields. (d) Temperature-dependent specific heat in the superconducting state ($H = 0$ kOe, open circles) and normal state ($H = 40$ kOe, filled up triangles) of $\text{Ti}_{1-x}\text{Mn}_x$ with $x = 0.12$. Solid lines show the fitting curves of specific heat in the superconducting state based on the s -wave model (red), d -wave model (green), and extended s -wave model (blue). (e) The ρ - T curves of $\text{Ti}_{1-x}\text{Mn}_x$ with $x = 0.12$ near the superconducting transition under different magnetic fields. (f) Upper critical fields (H_{c2}) versus T curves of $\text{Ti}_{1-x}\text{Mn}_x$ with $x = 0.12$. The fitting curves are based on the $\rho(T)$ data according to the GL theory (red line) and $C_p(T)$ data according to the WHH theory (green line).

more than 96% for $\text{Ti}_{1-x}\text{Mn}_x$ with $x = 0.12$ and 0.16, which further confirms the bulk superconductivity of the β phase in $\text{Ti}_{1-x}\text{Mn}_x$ alloys.

In order to determine the electron correlation strength in $\text{Ti}_{1-x}\text{Mn}_x$, we calculated the Wilson ratio (R_W) [48] of $\text{Ti}_{1-x}\text{Mn}_x$ with $x = 0.12$ by using the equation

$$R_W = \frac{4\pi^2 k_B^2}{3(g\mu_B)^2} \frac{\chi_0}{\gamma_n} = 7.28 \times 10^4 \frac{\chi_0}{\gamma_n}. \quad (2)$$

Here, χ_0 is the Pauli susceptibility arising from the electronic origin, which should be roughly temperature independent, γ_n is the specific-heat coefficient, g is the Landé factor, which takes about 2 for an electron, and μ_B is the Bohr magneton. The above equation gives a value of $R_W = 3.1$, being larger than 1 for free-electron approximation and about 1–2 for interacting Fermi liquid, implying a relatively strong electron correlation in $\text{Ti}_{1-x}\text{Mn}_x$ with the β phase.

Figure 6(e) presents the temperature-dependent resistivity under different magnetic fields of $\text{Ti}_{1-x}\text{Mn}_x$ with $x = 0.12$ near the superconducting transition. The T_c is gradually suppressed to low temperatures with increasing magnetic field,

and no superconducting transition could be observed down to 1.9 K when $H = 30$ kOe. Furthermore, the normal-state resistivities up to 30 kOe almost overlap with each other, indicating that the magnetoresistance of $\text{Ti}_{1-x}\text{Mn}_x$ with the β phase is negligible. The situation is different from that in the α -phase $\text{Ti}_{1-x}\text{Mn}_x$, in which negative magnetoresistance and minimal of resistivity are observed [32]. By using the criterion of temperature for reaching 50% of normal-state resistivity (ρ_{5K}), we can derive the value of T_c from ρ - T curves and present the results in Fig. 6(f). Usually, the temperature-dependent upper critical field (H_{c2}) could be described using the Ginzburg-Landau (GL) equation

$$H_{c2}(T) = H_{c2}(0) \frac{1 - t^2}{1 + t^2}, \quad (3)$$

where $t = T/T_c$. The fitting curve is shown as the red solid line in Fig. 6(f), which gives a value of $H_{c2}(0)$ about 62 kOe, and this value is much higher than its corresponding paramagnetic Pauli limit ($H_p = 1.84T_c = 44$ kOe for $T_c = 2.4$ K) [49]. $H_{c2}(0)$ can also be roughly estimated using the empirical formula $H_{c2}(0) = -0.693T_c \left(\frac{dH_{c2}}{dT}\right)_{T=T_c}$ in the dirty limit [50]

TABLE I. Superconducting and normal-state properties of $\text{Ti}_{1-x}\text{Mn}_x$.

Parameters	T_c (K)	γ_n mJ/(mol K ²)	$N(E_F)$ (states eV ⁻¹ f.u. ⁻¹)	β mJ/(mol K ⁴)	Θ_D (K)	$\Delta C/\gamma_n T _{T_c}$
$\text{Ti}_{0.88}\text{Mn}_{0.12}$	2.4(1)	5.55(1)	1.17(1)	0.047(2)	344(2)	1.44(6)
$\text{Ti}_{0.84}\text{Mn}_{0.16}$	1.9(1)	5.80(3)	1.23(2)	0.054(3)	328(5)	1.33(9)

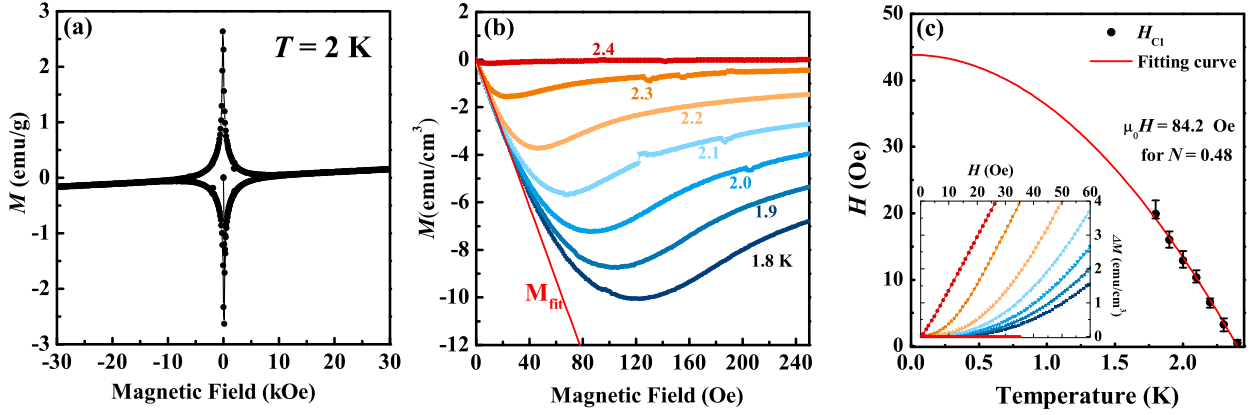


FIG. 7. (a) Magnetization hysteresis loop of $Ti_{1-x}Mn_x$ with $x = 0.12$ at 2 K. (b) Isothermal magnetization at different temperatures from 1.8 to 2.4 K. The red dashed line shows the linear fitting in the low-field region at 1.8 K. (c) Lower critical fields under different temperatures, and the fitting results according to Eq. (5). Inset illustrates the determination of $\mu_0 H_{c1}$.

as shown by the blue dashed line in Fig. 6(f). Taking $T_c = 2.4$ K, we can get a value of $H_{c2}(0) = 48$ kOe, still higher than the Pauli limit. However, according to the temperature dependence of heat-capacity data down to 0.4 K in Fig. 6(c), where the value of T_c is determined by entropy conservation, error bars correspond to the transition width. The upper critical field under low temperatures deviates from the predictions of the above two models. Surprisingly, the data could be well fitted using the Werthamer, Helfand, and Hohenberg (WHH) model [51,52], in a dirty limit for a superconductor with a single s -wave gap:

$$\ln \frac{1}{t} = \sum_{\nu=-\infty}^{\infty} \left\{ \frac{1}{|2\nu+1|} - \left[|2\nu+1| + \frac{\bar{h}}{t} + \frac{(\alpha_M \bar{h}/t)^2}{|2\nu+1| + (\bar{h} + \lambda_{so})/t} \right]^{-1} \right\}. \quad (4)$$

Here, $t = T/T_c$; $\bar{h} = 4H_{c2}(T)/(\pi^2 H' T_c)$, with $H' = |dH_{c2}/dT|_{T_c}$; λ_{so} is a parameter related to spin-orbit interaction; and α_M is the Maki parameter reflecting the strength of the spin paramagnetic effect. With the fitting parameters of $\alpha_M = 2.06$ and $\lambda_{so} = 0$, the data points that derived from heat capacity can be well fitted by Eq. (4) as the green solid line shown in Fig. 6(f). And the obtained value of $H_{c2}(0)$ is about 35 kOe, but such a value is obviously smaller than that of the Pauli limit field (44 kOe). We tend to believe that the value of H_{c2} extracted from heat-capacity data is more appropriate since it covers a wider range of temperatures to reveal the intrinsic property of $Ti_{1-x}Mn_x$ with $x = 0.12$. According to the GL theory, the obtained $H_{c2}(0)$ value can be used to estimate the coherence length $\xi_{GL}(0)$ at $T = 0$ K using the equation $H_{c2}(0) = \Phi_0/(2\pi \xi_{GL}^2)$, where $\Phi_0 = h/2e \approx 2.0678 \times 10^{-15}$ Wb is the magnetic flux quantum, and the coherent length $\xi_{GL}(0)$ is estimated to be 9.69 nm for $Ti_{1-x}Mn_x$ with $x = 0.12$.

Figure 7(a) presents the magnetization hysteresis loops of $Ti_{1-x}Mn_x$ with $x = 0.12$ at 2 K, which shows a typical behavior expected for type-II superconductors. To determine the lower critical field H_{c1} , we have performed the field dependence of magnetization (M - H) measurements at various

temperatures below the superconducting transition, as shown in Fig. 7(b). The red dashed line is the linear fit of the low-field region of the M - H curve at the lowest measured temperature in the present study (1.8 K), which can be recognized as the reference line describing the perfect diamagnetic state. Figure 7(c) plots the temperature dependence of lower critical field data of $Ti_{1-x}Mn_x$ with $x = 0.12$. The lower critical field was determined by using the criterion where the magnetization deviates from the linear fit of about 0.05 emu/cm³ [53], as shown in the inset of Fig. 7(c). The temperature-dependent lower critical field curve can be fitted with the equation

$$H_{c1}^*(T) = H_{c1}^*(0) \left[1 - \left(\frac{T}{T_c} \right)^2 \right], \quad (5)$$

yielding a zero-temperature $H_{c1}^*(0)$ of about 43.8 Oe with the T_c of about 2.4 K. Moreover, after considering the demagnetization effect by using the formula $H_{c1}(0) = H_{c1}^*(0)/(1-N)$, where N is the demagnetization factor with a value of 0.48, the corrected lower critical field $H_{c1}(0)$ is estimated to be 84.2 Oe.

The relatively small value of $H_{c1}(0)$ indicates that the quantized flux can easily enter the superconductor. The superconducting penetration depth λ_{GL} can be calculated through the obtained values of ξ_{GL} and $H_{c1}(0)$ by using the equation

$$H_{c1}(0) = \frac{\Phi_0}{4\pi \lambda_{GL}^2} \ln \frac{\lambda_{GL}}{\xi_{GL}}. \quad (6)$$

The calculated value of λ_{GL} is about 252.2 nm. The Ginzburg-Landau parameter is $\kappa_{GL} = \xi_{GL}/\lambda_{GL} = 26$, which is much larger than $1/\sqrt{2}$, indicating that $Ti_{1-x}Mn_x$ with the β phase is a type-II superconductor.

IV. DISCUSSION

Based on the data presented above, we argue that the superconducting component in $Ti_{1-x}Mn_x$ alloys originates from the β phase and the normal-state properties in the β phase show some unusual features. First, the magnetization and specific-heat measurements confirm the robust bulk superconductivity in the β phase. The filamentary superconductivity in the α

phase may originate from the residual component of the β phase in the matrix of the α phase. Second, the doping of Mn not only reduces the carrier density, but also changes the charge carrier of the material to a hole type as evident from the Hall resistivity measurements on $\text{Ti}_{1-x}\text{Mn}_x$ with $x = 0$ and 0.12. The effect of Mn doping on charge carriers and superconductivity in $\text{Ti}_{1-x}\text{Mn}_x$ with the β phase remains to be resolved. Third, the abnormal magnetic susceptibility behaviors, including the positive correlation between the magnetic susceptibility and temperature and the sudden drop of effective magnetic moment in the β -phase $\text{Ti}_{1-x}\text{Mn}_x$ with $x = 0.12$, indicate that the doping of Mn may introduce more magnetic interactions. In this case, the doping of magnetic Mn ions neither enhances the electronic density of states near the Fermi surface nor brings notable localized moment, but may lead to unexpected enhancement of superconductivity through possible antiferromagnetic spin fluctuations. More experimental results, such as neutron scattering and muon-spin rotation and relaxation ($\mu^+\text{SR}$) are expected in future work. If the spin fluctuations are proven to exist in the title system, the superconductivity in the β -phase $\text{Ti}_{1-x}\text{Mn}_x$ might have some unconventional origins since the magnetism-mediated unconventional superconductivity is often observed in some correlated system, such as cuprate [54], iron-pnictide [7,55], and heavy fermion superconductors [8,10]. However, the specific-heat data indicates that the superconductivity in the β phase possesses an s -wave gap, and the specific anomaly near T_c as well as the gap ratio $2\Delta/k_B T_c$ are close to the values predicted by the BCS theory in the weak-coupling limit. This raises the question, what is the role played by doping Mn atoms into the material? One possibility is that most of the Mn outer shell electrons join the conduction, leading to a small magnetic moment. Clearly, the correlation effect exists in the normal state of the β phase, as evidenced by the positive correlation between the magnetic susceptibility and temperature, together with the relatively large Wilson ratio.

Although we have conducted comprehensive investigations on the superconductivity of $\text{Ti}_{1-x}\text{Mn}_x$ alloys, there are still some interesting issues that need to be further clarified. For example, although filamentary superconductivity was observed in the α phase, one separated domelike superconducting region can always be seen in the phase diagram of $\text{Ti}_{1-x}\text{Mn}_x$ alloys as shown in Fig. 3(d) and Ref. [25]. And the onset transition temperature is even a bit higher than that of the β phase at higher doping levels. The superconductivity in the α phase might be due to the residual β phase embedded in the α phase, but the intrinsic α phase is not superconductive with better metallic behavior. Thus the origin of this domelike superconducting region in the α phase is still unsettled. Moreover, we recommend that the evolution of T_c of $\text{Ti}_{1-x}\text{Mn}_x$ alloys under high pressure is worth investigat-

ing. As we know, Ti undergoes a structural transformation sequence ($\alpha \rightarrow \omega \rightarrow \gamma \rightarrow \delta \rightarrow \beta$) under high pressures [29,56], and a dramatic pressure-enhanced superconductivity with the maximal T_c at about 26 K is achieved, which is the record high value among element superconductors. In the β phase of Ti (above 200 GPa), the T_c decreases with increasing pressure as evidenced by experimental data and theoretical calculations [30,31]. We also notice that in the β -phase Ti-V alloy, the T_c can be enhanced monotonically from about 7 K at ambient pressure to 18.2 K at 60 GPa without showing signatures of saturation upon increasing pressure [57]. Therefore, experiments on the superconductivity of $\text{Ti}_{1-x}\text{Mn}_x$ alloys under high pressure are highly desired and are actually underway. Our present study shows an unexpected full-volume superconductivity in the heavily Mn-doped $\text{Ti}_{1-x}\text{Mn}_x$ alloys, and provides a rich collection of properties of superconductivity as well as the normal state.

V. CONCLUSION

In summary, we have successfully synthesized $\text{Ti}_{1-x}\text{Mn}_x$ alloys with different Mn doping concentrations and measured their detailed physical properties. A transition from the α phase to the β phase was observed when the content of Mn exceeds 12 at. %, and the alloys exhibit bulk superconductivity in the β phase. Magnetic susceptibility, electrical resistivity, and specific-heat capacity measurements show that $\text{Ti}_{1-x}\text{Mn}_x$ with $x = 0.12$ (β phase) is a type-II superconductor with a Wilson ratio of about 3.1, suggesting a moderate electron correlation in the normal state. The low-temperature specific heat of $\text{Ti}_{1-x}\text{Mn}_x$ with $x = 0.12$ can be fitted by the s -wave gap with $2\Delta/k_B T_c = 3.6$ with a moderate pairing strength. Moreover, Hall resistivity measurements show that the charge carriers change from electron type in pure Ti metal to hole type in $\text{Ti}_{1-x}\text{Mn}_x$ with the β phase, and the value of carrier density decreases by an order of magnitude more than that of pure Ti, which suggests an interesting evolution of electronic properties via doping Mn. The possible evidence of the existence of spin fluctuations is proposed from the magnetization measurement, which may generate possible unconventional superconducting pairing in the β phase of $\text{Ti}_{1-x}\text{Mn}_x$.

ACKNOWLEDGMENTS

This work was supported by the National Key Research and Development Program of China (Grant No. 2022YFA1403201), National Natural Science Foundation of China (Grants No. 12204231, No. 11927809, and No. 12061131001), and the Strategic Priority Research Program of Chinese Academy of Sciences (Grant No. XDB25000000). Q.L. also acknowledges the support from the Jiangsu Shuangchuang program.

- [1] J. Bardeen, L. N. Cooper, and J. R. Schrieffer, *Phys. Rev.* **108**, 1175 (1957).
- [2] P. W. Anderson, *J. Phys. Chem. Solids* **11**, 26 (1959).
- [3] H. R. Khan and C. J. Raub, *Annu. Rev. Mater. Sci.* **15**, 211 (1985).

- [4] T. H. Geballe, B. T. Matthias, E. Corenzwit, and G. W. Hull, Jr., *Phys. Rev. Lett.* **8**, 313 (1962).
- [5] R. A. Hein, J. W. Gibson, B. T. Matthias, T. H. Geballe, and E. Corenzwit, *Phys. Rev. Lett.* **8**, 408 (1962).
- [6] B. T. Matthias, *Phys. Rev.* **97**, 74 (1955).

- [7] Y. Kamihara, T. Watanabe, M. Hirano, and H. Hosono, *J. Am. Chem. Soc.* **130**, 3296 (2008).
- [8] F. Steglich, J. Aarts, C. D. Bredl, W. Lieke, D. Meschede, W. Franz, and H. Schäfer, *Phys. Rev. Lett.* **43**, 1892 (1979).
- [9] Z. Ren, Q. Tao, S. Jiang, C. Feng, C. Wang, J. Dai, G. Cao, and Z. Xu, *Phys. Rev. Lett.* **102**, 137002 (2009).
- [10] S. S. Saxena, P. Agarwal, K. Ahilan, F. M. Grosche, R. K. W. Hasselwimmer, M. J. Steiner, E. Pugh, I. R. Walker, S. R. Julian, P. Monthoux, G. G. Lonzarich, A. Huxley, I. Sheikin, D. Braithwaite, and J. Flouquet, *Nature (London)* **406**, 587 (2000).
- [11] J. Cheng and J. Luo, *J. Phys.: Condens. Matter* **29**, 383003 (2017).
- [12] W. Wu, J. G. Cheng, K. Matsubayashi, P. P. Kong, F. K. Lin, C. Q. Jin, N. L. Wang, Y. Uwatoko, and J. L. Luo, *Nat. Commun.* **5**, 5508 (2014).
- [13] J.-G. Cheng, K. Matsubayashi, W. Wu, J. P. Sun, F. K. Lin, J. L. Luo, and Y. Uwatoko, *Phys. Rev. Lett.* **114**, 117001 (2015).
- [14] J. K. Bao, J. Y. Liu, C. W. Ma, Z. H. Meng, Z. T. Tang, Y. L. Sun, H. F. Zhai, H. Jiang, H. Bai, C. M. Feng, Z. A. Xu, and G. H. Cao, *Phys. Rev. X* **5**, 011013 (2015).
- [15] Z. T. Tang, J. K. Bao, Y. Liu, Y. L. Sun, A. Ablimit, H. F. Zhai, H. Jiang, C. M. Feng, Z. A. Xu, and G. H. Cao, *Phys. Rev. B* **91**, 020506(R) (2015).
- [16] Z.-T. Tang, J.-K. Bao, Z. Wang, H. Bai, H. Jiang, Y. Liu, H.-F. Zhai, C.-M. Feng, Z.-A. Xu, and G.-H. Cao, *Sci. China Mater.* **58**, 16 (2015).
- [17] Q. G. Mu, B.-B. Ruan, B.-J. Pan, T. Liu, J. Yu, K. Zhao, G. F. Chen, and Z. A. Ren, *Phys. Rev. B* **96**, 140504(R) (2017).
- [18] T. Liu, Q. G. Mu, B. J. Pan, J. Yu, B. B. Ruan, K. Zhao, G. F. Chen, and Z. A. Ren, *Europhys. Lett.* **120**, 27006 (2017).
- [19] W. Wu, K. Liu, Y. Li, Z. Yu, D. Wu, Y. Shao, S. Na, G. Li, R. Huang, T. Xiang, and J. Luo, *Natl. Sci. Rev.* **7**, 21 (2020).
- [20] C. Pei, P. Yang, C. Gong, Q. Wang, Y. Zhao, L. Gao, K. Chen, Q. Yin, S. Tian, C. Li, W. Cao, H. Lei, J. Cheng, and Y. Qi, *arXiv:2109.15213*.
- [21] T.-L. Hung, C.-H. Huang, L.-Z. Deng, M.-N. Ou, Y.-Y. Chen, M.-K. Wu, S.-Y. Huyan, C.-W. Chu, P.-J. Chen, and T.-K. Lee, *Nat. Commun.* **12**, 5436 (2021).
- [22] Z. Y. Liu, Q. X. Dong, P. T. Yang, P. F. Shan, B. S. Wang, J. P. Sun, Z. L. Dun, Y. Uwatoko, G. F. Chen, X. L. Dong, Z. X. Zhao, and J.-G. Cheng, *Phys. Rev. Lett.* **128**, 187001 (2022).
- [23] J. Hu, *Sci. Bull.* **61**, 561 (2016).
- [24] B. T. Matthias, G. W. Hull, E. Corenzwit, T. H. Geballe, and V. B. Compton, *Phys. Rev.* **128**, 588 (1962).
- [25] B. Matthias, V. B. Compton, H. Suhl, and E. Corenzwit, *Phys. Rev.* **115**, 1597 (1959).
- [26] B. T. Matthias and E. Corenzwit, *Phys. Rev.* **100**, 626 (1955).
- [27] M. C. Steele and R. A. Hein, *Phys. Rev.* **92**, 243 (1953).
- [28] R. L. Falge, Jr., *Phys. Rev. Lett.* **11**, 248 (1963).
- [29] A. Dewaele, V. Stutzmann, J. Bouchet, F. Bottin, F. Occelli, and M. Mezouar, *Phys. Rev. B* **91**, 134108 (2015).
- [30] X. Liu, P. Jiang, Y. Wang, M. Li, N. Li, Q. Zhang, Y. Wang, Y.-I. Li, and W. Yang, *Phys. Rev. B* **105**, 224511 (2022).
- [31] C. L. Zhang, X. He, C. Liu, Z. W. Li, K. Lu, S. J. Zhang, S. M. Feng, X. C. Wang, Y. W. Long, L. H. Wang, Y. Ye, V. B. Prakapenka, S. Chariton, Q. Li, Y. M. Ma, H. Z. Liu, C. F. Chen, and C. Q. Jin, *Nat. Commun.* **13**, 5411 (2022).
- [32] B. R. Hake, D. H. Leslie, and T. G. Berlincourt, *Phys. Rev.* **127**, 170 (1962).
- [33] J. A. Cape, *Phys. Rev.* **132**, 1486 (1963).
- [34] L. S. Chandra, M. K. Chattopadhyay, J. Chandra, M. A. Manekar, S. K. Pandey, R. Venkatesh, and S. B. Roy, *Supercond. Sci. Technol.* **31**, 085004 (2018).
- [35] F. Heiniger and J. Muller, *Phys. Rev.* **134**, A1407 (1964).
- [36] Z. Zhu, Y.-J. Zhang, Y. Li, Q. Li, W. Duan, and H.-H. Wen, *J. Phys.: Condens. Matter.* **34**, 475602 (2022).
- [37] K. Momma and F. Izumi, *J. Appl. Crystallogr.* **41**, 653 (2008).
- [38] R. M. Wood, *Proc. Phys. Soc.* **80**, 783 (1962).
- [39] J. Guo, G. Lin, S. Cai, C. Xi, C. Zhang, W. Sun, Q. Wang, K. Yang, A. Li, Q. Wu, Y. Zhang, T. Xiang, R. J. Cava, and L. Sun, *Adv. Mater.* **31**, 1807240 (2019).
- [40] P. Koželj, S. Vrtnik, A. Jelen, S. Jazbec, Z. Jagličić, S. Maiti, M. Feuerbacher, W. Steurer, and J. Dolinšek, *Phys. Rev. Lett.* **113**, 107001 (2014).
- [41] Y. Zhang, G. M. Stocks, K. Jin, C. Lu, H. Bei, B. C. Sales, L. Wang, L. K. Bland, R. E. Stoller, G. D. Samolyuk, M. Caro, A. Caro, and W. J. Weber, *Nat. Commun.* **6**, 8736 (2015).
- [42] R. I. Joseph and E. Schlömann, *J. Appl. Phys.* **36**, 1579 (1965).
- [43] Md. Matin, L. S. Sharath Chandra, S. K. Pandey, M. K. Chattopadhyay, and S. B. Roy, *Eur. Phys. J. B* **87**, 131 (2014).
- [44] S. Misawa, *Phys. Lett. A* **44**, 333 (1973).
- [45] Y. Nishihara, Y. Yamaguchi, M. Tokumoto, K. Takeda, and K. Fukamichi, *Phys. Rev. B* **34**, 3446 (1986).
- [46] Y. Nishihara, Y. Yamaguchi, T. Kohara, and M. Tokumoto, *Phys. Rev. B* **31**, 5775 (1985).
- [47] S. Jiang, H. Xing, G. Xuan, C. Wang, Z. Ren, C. Feng, J. Dai, Z. Xu, and G. Cao, *J. Phys.: Condens. Matter* **21**, 382203 (2009).
- [48] K. G. Wilson, *Rev. Mod. Phys.* **47**, 773 (1975).
- [49] A. M. Clogston, *Phys. Rev. Lett.* **9**, 266 (1962).
- [50] E. Helfand and N. R. Werthamer, *Phys. Rev.* **147**, 288 (1966).
- [51] N. R. Werthamer, E. Helfand, and P. C. Hohenberg, *Phys. Rev.* **147**, 295 (1966).
- [52] Y. Xiang, Q. Li, Y. Li, H. Yang, Y. Nie, and H.-H. Wen, *Chin. Phys. Lett.* **38**, 047401 (2021).
- [53] C. Ren, Z.-S. Wang, H.-Q. Luo, H. Yang, L. Shan, and H.-H. Wen, *Phys. Rev. Lett.* **101**, 257006 (2008).
- [54] P. A. Lee, N. Nagaosa, and X.-G. Wen, *Rev. Mod. Phys.* **78**, 17 (2006).
- [55] T. Oka, Z. Li, S. Kawasaki, G. F. Chen, N. L. Wang, and G.-Q. Zheng, *Phys. Rev. Lett.* **108**, 047001 (2012).
- [56] Y. Akahama, H. Kawamura, T. Le Bihan, *Phys. Rev. Lett.* **87**, 275503 (2001).
- [57] I. O. Bashkin, V. G. Tissen, M. V. Nefedova, and E. G. Ponyatovskii, *Phys. Solid State* **51**, 241 (2009).